frontiers | Frontiers in Aerospace Engineering

TYPE Original Research
PUBLISHED 12 January 2023
DOI 10.3389/fpace.2022.978261

OPEN ACCESS

EDITED BY
Yuncheng Du,
Clarkson University, United States

REVIEWED BY
Liangyu Zhao,
Beijing Institute of Technology, China
Zhiguo Yan,
Qilu University of Technology, China

*CORRESPONDENCE
Jie Shen,
shenjie74@163.com

†These authors have contributed equally to this work and share first authorship

SPECIALTY SECTION
This article was submitted to Intelligent Aerospace Systems, a section of the journal *Frontiers in Aerospace Engineering*

RECEIVED 25 June 2022
ACCEPTED 15 November 2022
PUBLISHED 12 January 2023

CITATION
Shen J, Dong Wq, Wang Z-f, Wang J, Wang Y, Liu Hm and Li H (2023), Negotiation of the global grid inspection UAV with random delay uncertainty in an information communication network based on a robust fault tolerance mechanism.
Front. Aerosp. Eng. 1:978261.
doi: 10.3389/fpace.2022.978261

Negotiation of the global grid inspection UAV with random delay uncertainty in an information communication network based on a robust fault tolerance mechanism

Jie Shen[1,2*†], Wen qi Dong[3†], Zhi-fang Wang[2], Jing Wang[1,3], Yang Wang[1], Han min Liu[3] and Haiyan Li[3]

[1]State Grid Jibei Zhangjiakou Wind and Solar Energy Storage and Transportation New Energy Co, Ltd., Beijing, China, [2]School of Electronics Engineering, Beijing University of Posts and Telecommunications, Beijing, China, [3]Hebei Province Wind and Solar Energy Storage Combined Power Generation Technology Innovation Center, Beijing, China

To accurately simulate the interference mechanism of information communication between unmanned aerial vehicles (UAVs) in the future global grid system, a type of control based on dynamic simulation of the satellite communication network and robust fault tolerance with a stochastic delay uncertain network system is proposed. Based on the imaginary future of the global energy Internet, with unknown information and communication interference, we established a UAV model from sensor to actuator network delay using a robust, fault-tolerant control algorithm and a satellite communication network model that combined the controller's mathematical model. The simulation results showed improved power transmission capability and communication coverage ability of UAVs by using the network fault-tolerant control mechanism with uncertain network delay and information communication interference. The stability and anti-interference performance was also significantly improved. This algorithm provides a strategy for the future development of global energy Internet.

KEYWORDS

power inspection UAV, information and communication interference, random time delay uncertain network, robust fault-tolerate control, extra-high voltage (EHV)

1 Introduction

With rapid economic globalization and transformation of energy structures, global energy Internet is developing as a main body of cross-regional transmission and transportation project construction. This Internet aims to promote global resource sharing, efficient energy, and clean energy development to promote construction of

the world's ecological civilization (Qing et al., 2009). These efforts have focused on the advancement and development of special high-voltage projects. Compared to EHV high-voltage transmission lines, the structure of UHVs is more complex (Liu, 2009), with higher specifications required in all aspects. Transmitted electrical energy from wind farms is connected to UHVs; however, grounded, wireless communication cannot cover wind farms and satellite communication rates cannot meet the requirements. Thus, the only feasible solution is to use UAV clusters for line patrol and inspection.

In long-term transmission line operation and maintenance, the timely detection and rapid elimination of security risks, to ensure safe and reliable line operation, is particularly important. UAVs have recently been used for power inspection to promote the development of new technology, guarantee its safety, ensure inspection quality, and improve inspection efficiency, with good results achieved.

Multi-rotor UAVs are mainly used at low-altitudes and in complex environments with obstacles such as cross-crossing lines, road bridges, buildings, and trees, as well as strong electromagnetic fields generated by UHV transmission lines, signals, and other unknown interference with information traffic. Failure to appropriately handle the UAV, the transmission line, and the surrounding environment can have consequences ranging from UAV crashes to personal and power grid security incidents, resulting in large-scale power outages. Therefore, study of the safety of using multi-rotor UAVs in proximity to UHV transmission lines is important (Xin-Zhe, 2012).

Actual flight drone control mainly faces two threats: hard killing and soft killing. Hard kill generally refers to physical destruction due to collision. In general, in soft killing, the most simple and rugged way is to interfere with UAV information and communication signals. Whether civil, commercial, or military, most UAVs face such interference. For the control of UAVs, transmission intensity is limited due to the transmission distance; moreover, the communication signal transmission strength from satellite or terrestrial base stations is relatively weak due to harsh natural environments and other unavoidable factors (Yong, 2013). Certain directional radio frequencies are likely to interfere with UAV information and communication transmission. Such signal interference prevents UAVs from obtaining accurate self-coordinates, leading to a lack of UAV control, which interrupts the inspection task (Fei, 2014). These effects constitute a long-range threat to UAVs.

UAVs will play an increasingly important role in electric power inspection, and efforts are in full swing to promote the development of methods to fight hard and soft killing and subsequent damage, which will become a new research field (Bouadi et al., 2008). The main focus of this study is soft and hard kill strategies to ensure that UAVs can maximize inspection tasks for further research simulation tests. The future of global grid UAV patrol is to provide a certain strategy (Ioannou and Sun, 1996).

The simulation in this study considered a four-rotor electric UAV as an example. This study proposes a robust, fault-tolerant control mechanism for information communication networks with stochastic delay uncertainties for UAV fleet systems for future global grid inspection. This mechanism ensured the stability of the UAV fleet flight control system when performing detection tasks in the face of different interference signals, and showed good anti-interference performance. Regarding partial and drift faults, the mechanism showed good fault tolerance performance when the actuator was interrupted. The physical structure of the model is shown in Figure 1.

2 Establishment of a mathematical model for an electric drilling four-rotor UAV

The spatial and body coordinate systems of the four-rotor UAV are shown in Figure 2.

Using Newton's second law, the dynamic model for a four-rotor aircraft can be expressed as follows:

$$\begin{cases} \dot{L} = v \\ m\ddot{L} = F_u - mg\dot{R} = RS(\lambda)I\dot{\lambda} = -\lambda \times I\lambda + F_u \end{cases} \tag{1}$$

Here, L is the distance from the four-rotor aircraft's center of mass to the space coordinate system *in situ*; m is the total quality of the four-rotor aircraft; F_u is the four-motor force; and λ is the four-motor aircraft relative to the body coordinate system of the rotating angular velocity, as follows (Hu, 2013):

$$I = \begin{bmatrix} I_{xx} & 0 & 0 \\ 0 & I_{yy} & 0 \\ 0 & 0 & I_{zz} \end{bmatrix} \tag{2}$$

In which the body revolves around three moments of inertia of the coordinate system for I_{xx}, I_{yy}, and I_{zz}.

R is the 3 × 3 order of direction cosine matrix obtained from the transformation matrix of the space coordinate system to the body:

$$\begin{cases} R_1 = \begin{bmatrix} \cos\theta\cos\psi \\ \cos\theta\sin\psi \\ \sin\theta \end{bmatrix} \\ R_2 = \begin{bmatrix} \cos\varphi\sin\psi + \sin\varphi\sin\theta\cos\psi \\ \cos\varphi\cos\psi + \sin\varphi\sin\theta\sin\psi \\ \sin\varphi\cos\theta \end{bmatrix} \\ R_3 = \begin{bmatrix} \sin\varphi\sin\psi + \cos\varphi\sin\theta\cos\psi \\ \sin\varphi\cos\psi + \cos\varphi\sin\theta\sin\psi \\ \cos\varphi\cos\theta \end{bmatrix} \end{cases} \tag{3}$$

FIGURE 1
Physical model of a four-rotor UAV.

The mathematical model of the space coordinates of the four-rotor aircraft is as follows:

$$\begin{cases} I_{xx}\ddot{\varphi} = \dot{\theta}\dot{\psi}\left(I_{yy} - I_{zz}\right) + lU_2 \\ I_{yy}\ddot{\theta} = \dot{\varphi}\dot{\psi}\left(I_{xx} - I_{zz}\right) + lU_3 \\ I_{zz}\ddot{\psi} = \dot{\theta}\dot{\varphi}\left(I_{xx} - I_{yy}\right) + U_4 \\ \begin{bmatrix} m\ddot{x} \\ m\ddot{y} \\ m\ddot{z} + mg \end{bmatrix} = \begin{bmatrix} \cos\varphi\cos\psi\sin\theta + \sin\varphi\sin\psi \\ \cos\varphi\sin\theta\sin\psi - \sin\varphi\cos\psi \\ \cos\varphi\cos\theta \end{bmatrix} \sum_{i=1}^{4} K_p\omega_i^2 \end{cases} \tag{4}$$

where l is the distance from the body geometry center to the center of the electrical installation, K_p is the lift coefficient, and ω_i is the rotating angular velocity. U_1, U_2, U_3, and U_4 for the four-motor control input angular velocity of the decision system are as follows:

$$\begin{bmatrix} U_1 \\ U_2 \\ U_3 \\ U_4 \end{bmatrix} = \begin{bmatrix} K_p & K_p & K_p & K_p \\ -K_p & 0 & K_p & 0 \\ 0 & -K_p & 0 & K_p \\ K_d & -K_d & K_d & -K_d \end{bmatrix} \begin{bmatrix} \omega_1^2 \\ \omega_2^2 \\ \omega_3^2 \\ \omega_4^2 \end{bmatrix} \tag{5}$$

3 Design of unmanned assemblies in the future global grid system

The use of unmanned aircraft for the inspection of transmission lines is just beginning. This technology mainly uses the UAV's modern flight control and image camera recognition for high-altitude long-range rapid detection of transmission lines. UAV-based power line patrol research involves several areas of high-tech collaborative applications, requiring a higher level of research and scientific research. However, compared to traditional methods, this method is more advanced, effective, and lower cost, ensuring safe operation of the line.

Figure 3 shows a block diagram of a hypothetical future grid system under UAV inspection (Wang et al., 2009).

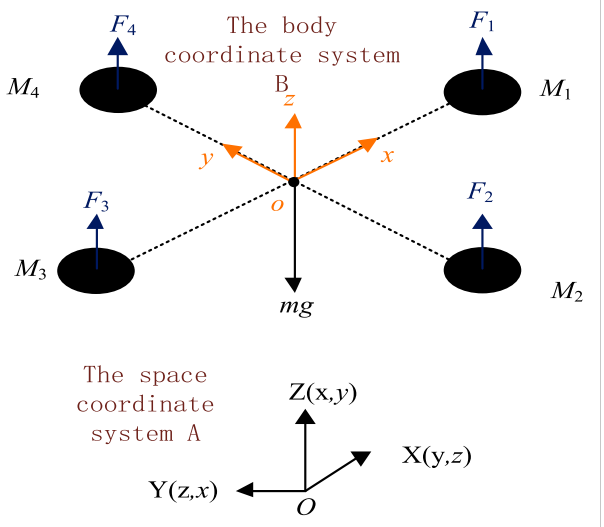

FIGURE 2
Four-rotor aircraft structure model diagram.

4 The establishment of an information communication interference model and its model for possible failure

According to the flight and dynamic characteristics of UAV aircrafts, we choose a robust, fault-tolerant control mechanism with stochastic uncertain time delay networks. The power line inspection process presents many uncertain factors which may delay operating characteristics. Robust control refers to a system affected by interference that maintains the desired performance. Adaptive control is a control method that can correct the characteristics of the system, allowing adaptation to changes in the dynamic characteristics of the object and external disturbances. A fault-tolerant control means that the system has a certain tolerance to faults in the event of an unknown failure; that is, lower sensitivity, to maintain performance indicators in the event of failure. By adopting robust adaptive fault-tolerant control, the performance of UAV systems can be well controlled. We also can improve their ability to resist hard and soft interference, increasing the information transmission and coverage abilities of UAVs (Zhang et al., 2014).

During inspection tasks, to facilitate accurate inspection of the object by confirmation, UAVs must upload high-definition photos or video, which requires a high-level camera as well as identification of location, as close as possible to the object being tested. However, as the UAV approaches the target, there are inevitable additional security risks. Hence, if the speed, altitude, and direction of the UAV are not controlled, it may impact the object, causing its failure. In other words, disturbances can occur during the task; such interference can be divided into hard kill jamming and soft kill jamming. Soft killing interference mainly

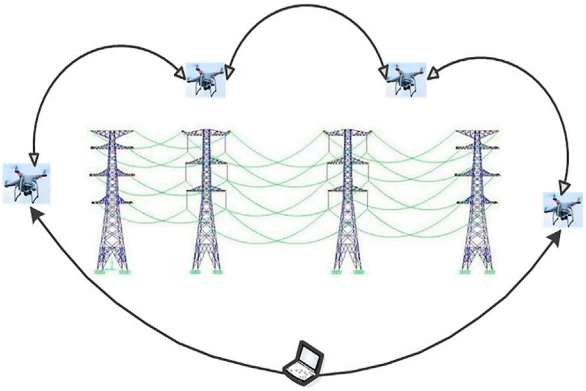

FIGURE 3
Demonstration block diagram of unmanned aerial vehicle group inspection.

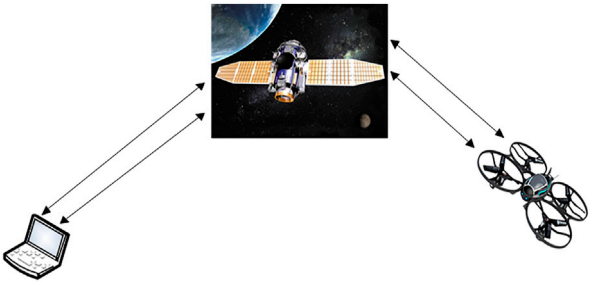

FIGURE 4
Future power grid system under control inspection by unmanned aerial vehicle effect map.

refers to interference in electronic information communication caused by electromagnetic interference due to high-voltage electricity (Mokhtari et al., 2005). In these situations, UAVs cannot be well controlled due to restrictions in information transmission and coverage capacities. Hard kill interference mainly refers to harsh environments such as strong winds and heavy rain, and physical interference such as physical damage due to collisions. In addition, "hard kill jamming" includes UAV actuator faults, comprising three types of actuator failure, partial failure, and drift fault (Yang et al., 2012).

A. Establishment of a hard-kill interference model

Let $g_i^f(t)$ say that the $i-th$ actuator is faulty. The comprehensive failure model is defined as follows (Khosravian and Namvar, 2012):

$$g_i^f(t) = [1-\rho_i(t)]g_i(t) + \Delta_i\Omega(t), i = 1, ..., m \tag{6}$$

where $\rho_i(t)$ is the unknown time-varying failure factor and Δ_i is an unknown constant. The upper and lower limits of the time-varying failure factor are expressed by the known constants $\overline{\rho_i}$ and ρ_i. According to the actual inspection situation encountered by the actuator during UAV flight, $0 \le \rho_i \le \overline{\rho_i} \le 1$. Importantly, when $\rho_i = \overline{\rho_i} = \Delta_i = 0$, the $i-th$ actuator is working normally; if $\rho_i = \overline{\rho_i} = 1, \Delta_i = 0$, the $i-th$ actuator has an interrupt fault; when $\rho_i \le \overline{\rho_i} \le 1, \Delta_i = 0$, the $i-th$ actuator has a partial failure; and when $\rho_i = \overline{\rho_i} = 0, \Delta_i = 1$, the $i-th$ actuator has drift faults. We use ε to represent the external harsh natural environment.

The following definitions are made:

$$g_i^f(t) = \left[g_1^f(t), ..., g_m^f(t)\right] = [I-\rho(t)]g(t) + \Delta\Omega(t) \tag{7}$$

Thus, $\rho(t) = \mathrm{diag}[\rho_1(t), ..., \rho_m(t)]$, $\Omega_t = [\Omega_1(t), ..., \Omega_n(t)]^T$, and $\rho_i(t) \in [\rho_i, \overline{\rho_i}]$.

The mathematical model (4) is expressed as the state space expression:

$$\begin{bmatrix} \dot{\theta} \\ \dot{\varphi} \\ \dot{\psi} \\ \ddot{\theta} \\ \ddot{\varphi} \\ \ddot{\psi} \end{bmatrix} = \begin{bmatrix} 0&0&0&1&0&0 \\ 0&0&0&0&1&0 \\ 0&0&0&0&0&1 \\ 0&0&0&0&0&0 \\ 0&0&0&0&0&0 \\ 0&0&0&0&0&0 \end{bmatrix} \begin{bmatrix} \theta \\ \varphi \\ \psi \\ \dot{\theta} \\ \dot{\varphi} \\ \dot{\psi} \end{bmatrix} + \mathrm{P} \begin{bmatrix} U_1 \\ U_2 \\ U_3 \\ U_4 \end{bmatrix} \tag{8}$$

Thus, $P = [P_{11} \;\; P_{12}]$ and

$$P_{11} = \begin{bmatrix} 0&0 \\ 0&0 \\ 0&0 \\ -\frac{k_{fc}l_1}{I_{yy}} & -\frac{k_{fc}l_1}{I_{yy}}\cos\omega \\ 0 & -\frac{k_{fc}l_1}{I_{xx}}\sin\omega \\ 0&0 \end{bmatrix}, P_{12} = \begin{bmatrix} 0&0 \\ 0&0 \\ 0&0 \\ -\frac{k_{fc}l_1}{I_{yy}}\cos\omega & 0 \\ -\frac{k_{fc}l_1}{I_{xx}}\sin\omega & 0 \\ 0 & -\frac{k_{fc}l_1}{I_{zz}} \end{bmatrix}$$

There is a state space expression in the case of a fault condition. The resulting system is as follows:

$$\begin{cases} \dot{x} = Ax + B_1[I-\rho(t)]g(t) + B_1\Delta\Omega(t) + B_2\varepsilon \\ y = Cx + D[I-\rho(t)]g(t) \end{cases} \tag{9}$$

Thus, B_1, B_2 is the appropriate dimension matrix. In addition, in the flight system model of UAV aircrafts in the event of failure, to ensure that the designed controller can achieve robust fault tolerance, the UAV flight control system makes the following assumptions (Zheng et al., 2014):

Supposition 1: All states within the system are observable.

Supposition 2: In the case of actuator failure, $\rho(t) \in \Delta_{\rho(t)}(t)$ and all $\{A \;\; B_1[I-\rho(t)]\}$ are controllable.

Supposition 3: In the actuator failure mode, the control system of the whole UAV satisfies the following condition:

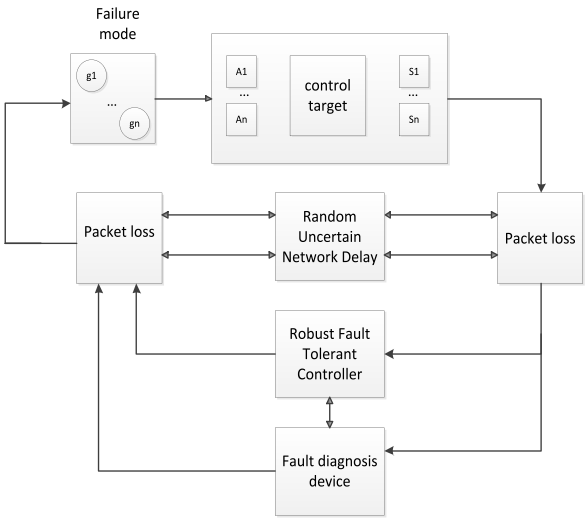

FIGURE 5
Robust fault-tolerant mechanism for uncertain networks with random delay.

$$\operatorname{rank}(B_1) = \operatorname{rank}(B_1(I - \rho(t))) \tag{10}$$

Supposition 4: All actuators of the UAV can fail at the same time.

B. Establishment of a soft-kill interference model

UAVs are likely to encounter electromagnetic interference caused by high voltage during near- or even long-distance power patrol inspection, which leads to uncontrolled UAV flight. Therefore, the study of how to reverse information and communication interference requires the establishment of a corresponding mathematical model so that the UAV can perform the corresponding patrol task better (Yan, 2013).

The dry signal ratio in the interference equation is used to determine the target receiver. To obtain a dry signal ratio, the signal and interference power values at the receiving device are first calculated (Zheng et al., 2013). The signal power P_s at the receiving device is:

$$P_s = \frac{P_{Ts} G_{Ts} G_{Rs}}{L} \tag{11}$$

where P_{Ts} is the signal power output for the transmitting device, G_{Ts} is the antenna gain for the direction of the communication-transmitting device to the target receiving device, and G_{Rs} is the path consumption of the target receiving device to the communication device.

The interference power at the target receiving device P_j is:

$$P_j = \frac{P_{Tj} G_{Tj} G_{Rj}}{L} \cdot F_b \cdot p \tag{12}$$

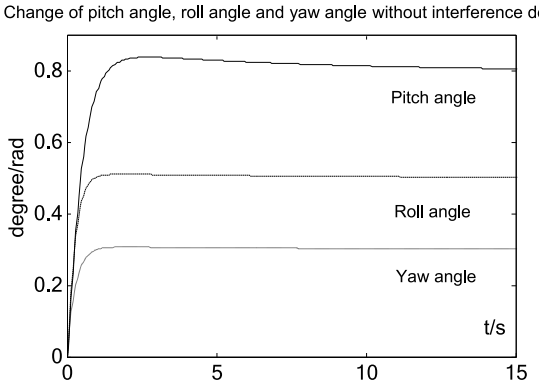

FIGURE 6
Changes in the pitch, roll, and yaw angles without interference.

where P_{Tj} is the interfering power, G_{Tj} is the antenna gain for the interference device to the receiving device, G_{Rj} is the antenna gain of the target receiving device to the interference device, L_j is the path consumption for the interference device to the receiving device, F_b is the filter consumption, and p is the consumption for polarization.

Filter loss is defined as the power loss caused by the filter that occurs because the receiving device uses a band-pass filter to filter the interference signal of the partial frequency. When the interference signal bandwidth is larger than the useful signal bandwidth, or when the interference signal deviates from the useful signal, the filter will transmit a signal outside its operating frequency. As interference is filtered out, its role will weaken. The following reflects the proportion of interference power to the total power of the UAV:

$$F_b = w_n / W_n \tag{13}$$

where w_n is the interference width of the interfering signal entering the receiving device and W_n is the interference spectrum width.

When the entire spectrum of the interference signal passes through the bandpass filter, $F_b = 1$.

Polarization loss is defined as the loss caused by the difference in the polarization direction of the interfering wave emitted by the interfering transmitting device and the receiving antenna. This loss can be expressed by p, which is the loss coefficient: $0 \le p \le 1$.

The control effect when the UAV is controlled remotely is shown in Figure 4.

The dry signal ratio, $\frac{P_j}{P_s} = \frac{P_{Tj} G_{Tj} G_{Rj} L_s}{P_{Ts} G_{Ts} G_{Rs} L_j} \cdot F_b \cdot p$, is called the airspace communication interference equation (Wang et al., 2021a; Wang et al., 2021b).

From the above equation, the dry signal ratio is related to filter and polarization losses and also to the signal (useful and

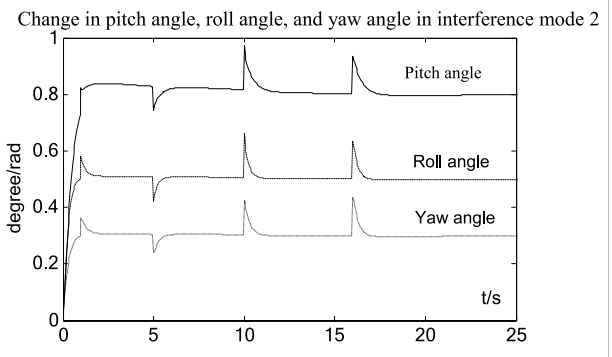

FIGURE 7
Interference pattern 1, with changes in the pitch, roll, and yaw angles.

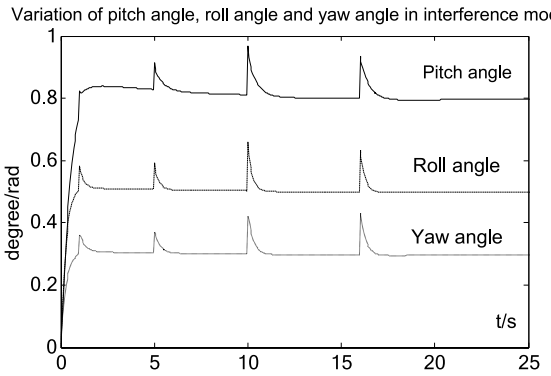

FIGURE 8
Interference pattern 2, with changes in the pitch, roll, and yaw angles.

interference signals) transmit power, two sets of antenna gain, and two path losses (Wang and Fu, 2017).

According to the definition of the pressing coefficient k_γ, when the jamming is effective, the dry signal ratio of the UAV should be satisfied: $\frac{P_j}{P_s} \geq k_\gamma$. At this time, the interference can effectively suppress the communication of the target signal. Only when the pressing coefficient of the UAV flight communication system is known, can the jamming power be estimated using the communication disturbance equation. It can be expressed in decibels as follows:

$$P_{Tj\,(\mathrm{dB})} \geq P_{Ts\,(\mathrm{dB})} + A_{z\,(\mathrm{dB})} + B_{z\,(\mathrm{dB})} - C_{z\,(\mathrm{dB})} + 10\lg k_\gamma \tag{14}$$

In this formula, the following equation should be satisfied:

$$\begin{cases} A_z = \left[(G_{Ts} + G_{Rs}) - \left(G_{Tj} + G_{Rj} \right) \right] \\ B_z = \left[L_j - L_s \right] \\ C_z = \left[F_b + p \right] \end{cases} \tag{15}$$

However, when calculating the interference power, the spectrum width of the interference signal entering the UAV receiving device is usually not determined; thus, in practice, the following formula is commonly used to calculate the filter loss:

$$P_{Tj} \geq P_{Ts} \cdot \frac{G_{Ts} G_{Rs} L_j}{G_{Tj} G_{Rj} L_s} \cdot \frac{k_\gamma}{F_b \cdot p} \tag{16}$$

The polarization loss p is difficult to determine; when estimated, it can be considered as the design capacity: $F_b = \frac{B_R}{B_j}$.

In which B_R is the UAV receiver bandwidth and B_j is the interference device bandwidth (Tang and Dai, 2013).

The path loss difference is generally given by:

$$\left(L_j - L_s \right)_{(\mathrm{dB})} = 20\lg\left(\frac{\gamma_i}{\gamma_s} \right) + 20\lg\left(\frac{W_s}{W_j} \right) \tag{17}$$

In which W_j is the attenuation factor for the effective information communication path and W_j is the attenuation factor for the interference path.

To estimate the interference distance in the future grid system, the communication interference equation should first be used to estimate the path loss (Wang and Xiao-Ning, 2012):

$$\left[L_j - L_s \right]_{(\mathrm{dB})} \leq A_{x\,(\mathrm{dB})} + B_{x\,(\mathrm{dB})} + C_{x\,(\mathrm{dB})} - 10\lg k_\gamma \tag{18}$$

In which

$$\begin{cases} A_x = \left[P_{Tj} - P_{Ts} \right] \\ B_x = \left[(G_{Tj} + G_{Rj}) - (G_{Ts} + G_{Rs}) \right] \\ C_x = \left[F_b + p \right] \end{cases} \tag{19}$$

Then, we can estimate the interference action distance using a general expression of the path loss difference. That is:

$$\frac{L_j}{L_s} \leq \frac{P_{Tj} G_{Tj} G_{Rj}}{P_{Ts} G_{Ts} G_{Rs}} \cdot \frac{F_b \cdot p}{k_\gamma} \tag{20}$$

When the LEO satellite communicates with multiple UAVs, a collision-limitation algorithm can be used. In general, when the ratio of the number of code channels to the total number of code channels of the UAV license-free system is $\frac{\sqrt{A_x}}{\sqrt{A_x}+\sqrt{B_x}}$, the system can obtain the maximum throughput.

5 Robust fault-tolerant control mechanism for stochastic uncertain network delays during power inspection by unmanned aerial vehicles

In this section, the system control mechanism block diagram is shown in Figure 5, in which the UAV sensor is time-driven work, while the controller and actuator are task-driven work (Wang et al., 2020).

Here, $\tau_1(t)$ represents the network delay from the sensor to the controller and $\tau_2(t)$ represents the network delay from the

TABLE 1 Transmission capacity and coverage of the indicators of the assessment results.

Serial number	Indicator name	Index weight	Index value	Indicator evaluation value
1	Uplink rate	0.1666666667	2,000,000	0.25819888974716115
2	Downlink rate	0.1666666667	10,000,000	0.447213595499958
3	Number of bands	0.1666667	5	0.99995720062048155
4	Communication bandwidth	0.1666666667	2500	0.67295752284617727
5	Number of modulation methods	0.1666666667	1	0.331259695023578
6	Number of encoding methods	0.1666666667	1	0.331259695023578
7	Covering the average duration	0.25	−1	0
8	Percentage of coverage	0.25	−1	0
9	Continuous coverage over an average duration	0.25	−1	0
10	Coverage interval average duration	0.25	−1	0
11	Percentage of covered area	0.5	−1	0
12	Coverage multiplicity	0.5	−1	0

controller to the actuator. If we suppose that $\tau_1(t)$, $\tau_2(t)$ is an arbitrary random Markov chain, denoted by $\tau_1(\eta_1(t))$, $\tau_2(\eta_2(t))$, where $\eta_1(t)$, $\eta_2(t)$ is the random time of the discrete-time Markov process representing the modal of the network delay, then the corresponding finite state set is $S_1 = \{1, 2, ..., N_1\}$ and $S_2 = \{1, 2, ..., N_2\}$. Here, $\eta_1(t)$ corresponds to the transition probability matrix $\Pi_1 = (\pi_{1ij}) \in R^{N_1 \times N_1}$, which is defined as follows:

$$P\{\eta_1(t+\Delta) = j \,|\, \eta_1(t) = i\} = \begin{cases} \pi_{1ij}\Delta + o(\Delta), i \neq j \\ 1 + \pi_{1ij}\Delta + o(\Delta), i = j \end{cases}$$

In this formula, $\lim_{\Delta \longrightarrow 0} [o(\Delta)/\Delta] = 0$, π_{ij} is the jump from status i to status j. When $i \neq j$, $\pi_{ij} \geq 0$ and $\pi_{ij} + \sum_{i \neq j, j=1}^{N_1} \pi_{ij} = 0$ holds true. Similarly, the transition probability matrix of $\eta_2(t)$ is $\Pi_2 = (\pi_{2ij}) \in R^{N_2 \times N_2}$ and is defined as follows:

$$P\{\eta_2(t+\Delta) = j \,|\, \eta_2(t) = i\} = \begin{cases} \pi_{2ij}\Delta + o(\Delta), i \neq j \\ 1 + \pi_{2ij}\Delta + o(\Delta), i = j \end{cases}$$

Assuming that the state of the UAV control system considered above is observable *via* the sensor (Wang et al., 2022a), we can design the following state-dependent feedback controller that relies on the sensor-to-actuator network delay:

$$u_T(t) = K[\eta_1(t)]x\{t - \tau_1[\eta_1(t)] - \tau_2[\eta_2(t)]\} \tag{21}$$

where $u(t) \in R^q$ is the control input to the actuator and $K(\eta(t))$ is the fault tolerance control rate to be obtained; $\eta_1(t) \in S_1, \eta_2(t) \in S_2$.

First, we consider the delay in the future power grid inspection, assuming that the interference will cause a time delay in the control of UAVs performing the inspection. In this case, using the comprehensive application of formula (9), the delay closed-loop control system can be used to detect the interference of the UAV:

$$\begin{cases} \dot{x}(t) = Ax(t) + B_1 Mu_T(t) + B_1 \Delta\Omega(t) + B_2 \varepsilon(t) \\ y(t) = Cx(t) + DMu_T(t) \\ x(t) = \Phi(t), \eta_1(t) = \eta_{10}, \eta_2(t) = \eta_{20}, t \in [-\bar{\delta}, 0] \end{cases} \tag{22}$$

where M is the appropriate dimension matrix, the initial condition $\Phi(t)$ is the continuous initial vector function on $[-\bar{\delta}, 0]$, and η_{10}, η_{20} are the initial probability distributions of $\eta_1(t), \eta_2(t)$, respectively.

In addition, considering potential system failure, we use $u_g(t) = Mu(t)$ to indicate a fault in the input signal, and then consider uncertainty in the future power inspection situation, including unexpected situations such as poor natural conditions (Wang et al., 2009), (Wang et al., 2022a), (Wang et al., 2021a). Thus, such uncertainties in the environment, as well as other factors, and their impacts on information and communication interference must be considered. The stochastic closed-loop control system under such uncertain factors is:

$$\begin{cases} \dot{x}(t) = A_b(t)x(t) + B_{1b}(t)Mu_g(t) + B_{1b}(t)\Delta\Omega(t) + B_2\varepsilon(t) \\ y(t) = Cx(t) + DMu_g(t) \\ x(t) = \Phi(t), \eta_1(t) = \eta_{10}, \eta_2(t) = \eta_{20}, t \in [-\bar{\delta}, 0] \end{cases} \tag{23}$$

where $A_b(t) = A + \Delta A(t)$, $B_{1b} = B_1 + \Delta B_1(t)$, and $\Delta A(t), \Delta B_1(t)$ represent the time-varying real-valued matrices of the UAV in the event of uncertainty, respectively, and $F(t)$ should satisfy $F^T(t)F(t) \leq I$. We also make the following assumption: $[\Delta A \ \ \Delta B_1] = HF(t)[V_1 \ \ V_2]$, where H, V_1, V_2 is the real constant matrix of the appropriate dimension.

Finally, combined with the above two cases, (9), (21), (22), and (23) can be obtained by inspection of UAVs in the soft kill

the hard kill auxiliary interference situations under the random uncertain network. The delayed closed-loop control system is as follows:

$$\begin{cases} \dot{x}(t) = \bar{A}x(t) + \overline{B_1}Mu_T(t) + \overline{B_1}\Delta\Omega(t) + B_2\varepsilon(t) \\ y(t) = Cx(t) + DMu_T(t) \\ x(t) = \Phi(t), \eta_1(t) = \eta_{10}, \eta_2(t) = \eta_{20}, t \in \left[-\bar{\delta}, 0\right] \end{cases} \tag{24}$$

In this formula, $\bar{A} = A + HF(t)V_1$ and $\bar{B} = B_1 + HF(t)V_2$.

The robust fault-tolerant control mechanism for the UAV stochastic uncertain network delay control system is defined as follows:

Definition 5.1. When $\equiv 0$, for the initial state $\Phi(t), t \in [-\bar{\delta}, 0]$, the network delay initial mode $\eta_1 \in S_1$, $\eta_2 \in S_2$, if there is a positive number $\Psi(\Phi, \eta_1, \eta_2)$ so that

$$\lim_{T \longrightarrow \infty} \omega\left[\int_0^T \|x(s)\|^2 \mathrm{d}s\right] \le \Psi(\Phi, \eta_1, \eta_2) \tag{25}$$

and system 3 is stochastic and stable.

Definition 5.2. Under the zero initial conditions, suppose $\gamma > 0$, for any non-zero external disturbance input $\varepsilon(t) \in L_2[0, \infty)$, if satisfied by:

$$\omega\int_0^\infty z^T(t)z(t)\mathrm{d}t \le \gamma^2\omega\int_0^\infty \varepsilon^T(t)\varepsilon(t)\mathrm{d}t \tag{26}$$

Thus, system 3 satisfies the H_∞ performance suppressed by the external disturbance γ.

In addition, we give the following lemmas to ensure that the design of a stochastic uncertain network delay robust fault-tolerant controller is stable and reliable.

Lemma 5.1. Given that any fitness matrix $Y = Y^T$, R_1, R_2, and U are positive definite diagonal matrices, for all time-dependent fitness matrices $\sum(t)$ satisfying $\|\sum(t)\| \le U$, the sufficient and necessary condition for the inequality $Y + R_1\sum(t)R_2 + R_2^T\sum^T(t)R_1^T < 0^T(t)$ to be established is that there exists a constant $\kappa > 0$ such that the following inequality holds:

$$Y + \kappa R_1 U R_1^T + \kappa^{-1} R_2^T U R_2 < 0 \tag{27}$$

Lemma 5.2. Given the appropriate dimension matrix Z, G and matrix $P = P^T > 0$, the following inequality holds:

$$-G^T P^{-1} G \le Z^T P Z - G^T Z - Z^T G \tag{28}$$

The results of H_∞ performance and stability analysis of the stochastic uncertain network delay robust fault-tolerant control systems under UAV actuator failure are given.

Theorem 5.1. For the given positive numbers $\gamma, \eta_1 \in S_1$ and $\eta_2 \in S_2$, if the matrix $P(\eta_1, \eta_2) = P^T(\eta_1, \eta_2) > 0$, $R_1 = R_1^T > 0$ and

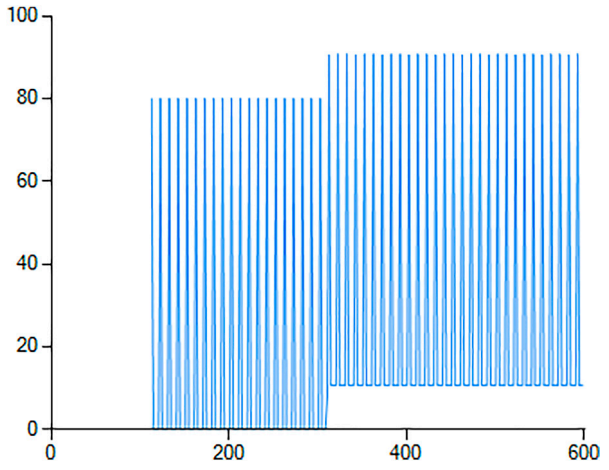

FIGURE 9
Network throughput graph.

$R_2 = R_2^T > 0$, and the controller $K(t)$ satisfies the following conditions, the following matrix inequality is established:

$$\begin{bmatrix} \prod_1(\eta_1, \eta_2) & * & * & * & * \\ A_1 & -R_1 - d_{\eta_1\eta_2}R_2 & * & * & * \\ E^T P(\eta_1, \eta_2) & 0 & -\gamma I & * & * \\ C & DMK(t) & 0 & -\gamma I & * \\ R_2 A & R_2 BMK(t) & R_2 E & 0 & -\mu_{\eta_1\eta_2}^{-1} R_2 \end{bmatrix} < 0 \tag{29}$$

where

$$\begin{cases} A_1 = BMK(t)P(\eta_1, \eta_2) + d_{\eta_1\eta_2}R_2 \\ \Pi_1(\eta_1, \eta_2) = A^T P(\eta_1, \eta_2)A + \sum_{j=1}^{N_1}\pi_{1ij}P(j, \eta_2) + \sum_{j=1}^{N2}\pi_{2ij}P(\eta_1, j) \\ \mu_{\eta_1\eta_2} = \left[(\tau_1(\eta_1)) + (\tau_2(\eta_2)) + 0.5(\alpha + \beta)(\overline{\delta^2} - \delta^2)\right] \\ d_{\eta_1\eta_2} = \left[(\tau_1(\eta_1)) + (\tau_2(\eta_2))\right]^{-1} \end{cases}$$

Thus, the systematic (21) is stochastic and satisfies H_∞ performance.

Proof: Define a random process $\{x(t), \tau_1(\eta_{1t}), \tau_2(\eta_{2t})\}$ that satisfies $x(t) = x(t+s)$, $s \in [-\tau_1(\eta_{1t}) - \tau_2(\eta_{2t}), 0]$. In addition, as η_{1t} and η_{2t} denote $\eta_1(t)$ and $\eta_2(t)$, respectively, then the random process can be a strong Markov process. The following Lyapunov–Krasovskii function is constructed: $V(x_t, \eta_{1t}, \eta_{2t}) = V_0(x_t, \eta_{1t}, \eta_{2t}) + V_1(x_t, \eta_{1t}, \eta_{2t}) + V_2(x_t, \eta_{1t}, \eta_{2t})$, $V_0(x_t, \eta_{1t}, \eta_{2t}) = x^T(t)P(\eta_{1t})x(t)$, and it satisfies $P(\eta_{1t}, \eta_{2t}) > 0 (\eta_{1t} \in S_1, \eta_{2t} \in S_2)$, $R_1, R_2 > 0$, and

$$V_1(x_t, \eta_{1t}, \eta_{2t}) = \int_{t-T_1(\eta_1)-T_2(\eta_2)}^{t} V_{1a}(s)ds + (\alpha + \beta)\int_{-\bar{\delta}}^{-\delta}\int_{t+\vartheta}^{t} V_{1b}(s)ds d\vartheta$$

where

$$V_{1a}(s) = x^T(s)R_1x(s),\ V_{1b}(s) = \dot{x}^T(s)R_1\dot{x}(s)$$

$$V_2(x_t,\eta_{1t},\eta_{2t}) = \int_{t-T_1(\eta_1)-T_1(\eta_2)}^{t}\int_{t+\vartheta}^{t} V_{2a}(s)ds + (\alpha+\beta)\int_{-\delta}^{-\delta}\int_{t+\vartheta}^{t} V_{2b}(s)dsd\vartheta$$

$$V_{2a}(s) = \dot{x}^T(s)R_2\dot{x}(s)V_{2b}(s) = \dot{x}^T(s)R_2\dot{x}(s)(s-t-\vartheta)$$

Let $\eta_{1t}=a, \eta_{2t}=b$. We obtain the weak infinitesimal operators (Yan, 2013) of the functions $V_0(x_t,a,b), V_1(x_t,a,b), V_2(x_t,a,b)$, along the state trajectory of system (3) to obtain the weak infinitesimal operator of $V(x_t,a,b)$:

$$\begin{aligned}
&\angle V(x_t,a,b) \le x^T(t)P(a,b)(Ax(t)+BMK(t)\times x(t-\tau_1(a)-\tau_2(b)))\\
&+(Ax(t)+BMK(t)x(t-\tau_1(a)-\tau_2(b)))^TP(a,b)x(t)\\
&+\sum_{j=1}^{N_1}\pi_{1ij}x^T(t)P(j,b)x(t)+\sum_{j=1}^{N_2}\pi_{2ij}x^T(t)P(a,j)x(t)\\
&+\sigma x^T(t)R_1x(t) = x^T(t-\tau_1(\eta_1)-\tau_2(\eta_2))R_1x(t-\tau_1(\eta_1)-\tau_2(\eta_2))\\
&+\mu_{ab}V_a^T(t)R_2V_a(t)+d_{ab}\xi^T(t)\begin{bmatrix}-R_2 & R_2\\ R_2 & -R_2\end{bmatrix}\xi(t)\\
&=\xi^T(t)N(a,b)\xi(t)
\end{aligned}$$

where

$$V_a(t) = Ax(t)+BMK(t)\times x(t-\tau_1(a)-\tau_2(b))$$

and

$$N(a,b) = \begin{bmatrix}\prod_1(a,b) & P(a,b)BMK(t)+d_{ab}R_2\\ (BMK(t)P(a,b)+d_{ab}R_2) & -R_1-d_{ab}R_2\end{bmatrix} + \mu_{ab}\begin{bmatrix}A & BMK(t)\end{bmatrix}^TR_2\begin{bmatrix}A & BMK(t)\end{bmatrix}$$

According to Schur refraction, $N(a,b)<0$ holds true by Eq. 29. Let $\chi = \min_{a\in S_1, b\in S_2}\lambda_{\min}(-N(a,b))$, according to the weak infinitesimal operator of $V(x_t,a,b)$ and Dynkin (Wang and Xiao-Ning, 2012).

$$\begin{aligned}
&\kappa[V(x(T),\eta_1(T),\eta_2(T))]-\kappa[V(x_0,\eta_{10},\eta_{20})]\\
&=\kappa\left[\int_0^T\angle V(x(s),\eta_1(s),\eta_2(s))ds\right] \le -\chi\kappa\left(\int_0^T\|x(s)\|^2ds\right)
\end{aligned}$$

When $T\to\infty$, the above inequality holds at both ends of the limits,

$$\begin{aligned}
&\lim_{T\longrightarrow\infty}[V(x(T),\eta_1(T),\eta_2(T))]-\kappa[V(x_0,\eta_{10},\eta_{20})]\\
&\le -\chi\lim_{T\longrightarrow\infty}\kappa\left(\int_0^T|x(s)|^2ds\right)
\end{aligned}$$

because $\lim_{T\longrightarrow\infty}\kappa[V(x(T),\eta_1(T),\eta_2(T))]\ge 0$ and

$$\begin{aligned}
&\lim_{T\longrightarrow\infty}\kappa\left(\int_0^T|x(s)|^2ds\right)\le\chi^{-1}\kappa[(x_0,\eta_{10},\eta_{20})]\\
&=\Psi(\Phi,\eta_{10},\eta_{20})
\end{aligned}$$

According to Definition 5.1, system (24) is randomly stable.

Thus, system (24) satisfies the H_∞ performance γ. Under the zero initial condition, the Lyapunov–Krasovskii function is combined with the weak infinitesimal operator of $V(x_t,a,b)$ to establish the following equation:

$$\dot{x}(t) = Ax(t)+BMK(t)\dot{x}[t-\tau_1(\eta_1(t))-\tau_2(\eta_2(t))]+Ew(t)$$

Therefore,

$$\angle V(x_t,\eta_{1t}=a,\eta_{2t}=b)\le\zeta^T(t)\Xi_1(a,b)\zeta(t) \tag{30}$$

In this equation, $\zeta(t) = [\,\xi^T(t)\ \ w^T(t)\,]^T$ and

$$\begin{aligned}
&\Xi_1(a,b) =\\
&\begin{bmatrix}\Pi_1(a,b) & P(a,b)BMK(t)+d_{ab}R_2 & PE\\ (BMK(t))^TP(a,b)+d_{ab}R_2 & -R_1-d_{ab}R_2 & 0\\ E^TP & 0 & 0\end{bmatrix}\\
&+\mu_{ab}[\,A\ \ BMK(t)\ \ E\,]^TR_2[\,A\ \ BMK(t)\ \ E\,]
\end{aligned}$$

The following functional indicators are defined:

$$J = \varepsilon\left\{\int_0^\infty[\gamma^{-1}z^T(t)z(t)-\gamma\omega^T(t)\omega(t)]dt\right\} \tag{31}$$

Under the zero initial conditions:

$$V(x_0,\eta_{10},\eta_{20}) = 0,\quad V(x(\infty),\eta_1(\infty),\eta_2(\infty))\ge 0$$

From Dynkin's formula we get,

$$\begin{aligned}
J &= \varepsilon\left\{\int_0^T[\gamma^{-1}z^T(t)z(t)-\gamma\omega^T(t)\omega(t)+\angle V(x_t,a,b)]dt\right\}\\
&\quad -V(x(\infty),\eta_1(\infty),\eta_2(\infty))\\
&\le\varepsilon\left\{\int_0^\infty[\gamma^{-1}z^T(t)z(t)-\gamma\omega^T(t)\omega(t)+\angle V(x_t,a,b)]dt\right\}
\end{aligned} \tag{32}$$

Inserting (27) into (29), we get:

$$\begin{aligned}
&\gamma^{-1}z^T(t)z(t)-\gamma w^T(t)w(t)+\angle V(x_t,t,a,b)\\
&\le\xi^T(t)\gamma^{-1}[\,C\ \ DMK(t)\,]^T[\,C\ \ DMK(t)\,]\xi(t)\\
&-\gamma w^T(t)w(t)+\zeta^T(t)\Xi_1(a,b)\zeta(t)\\
&\le\zeta^T(t)\Xi_2(a,b)\zeta(t)
\end{aligned} \tag{33}$$

In this equation,

$$\begin{aligned}
&\Xi_2(a,b) =\\
&\begin{bmatrix}\Pi_1(a,b) & P(a,b)BMK(t)+d_{ab}R_2 & PE\\ (BMK(t))^TP(a,b)+d_{ab}R_2 & -R_1-d_{ab}R_2 & 0\\ E^TP & 0 & -\gamma I\end{bmatrix}\\
&+\mu_{ab}[\,A\ \ BMK(t)\ \ E\,]^TR_2[\,A\ \ BMK(t)\ \ E\,]\\
&+\gamma^{-1}[\,C\ \ DMK(t)\ \ 0\,]^T\times[\,C\ \ DMK(t)\ \ 0\,]
\end{aligned}$$

According to the Schur refute (Tang and Dai, 2013), when equation (4.1) is equivalent to $\Xi_2(a,b)<0$, it holds; thus, for all $w(t)\in L_2[\,0\ \ \infty\,)$, when $\zeta(t)\neq 0$, the following inequality is true:

$$\gamma^{-1}z^T(t)z(t)-\gamma w^T(t)w(t)+\angle V(x_t,t,a,b)<0 \tag{34}$$

and

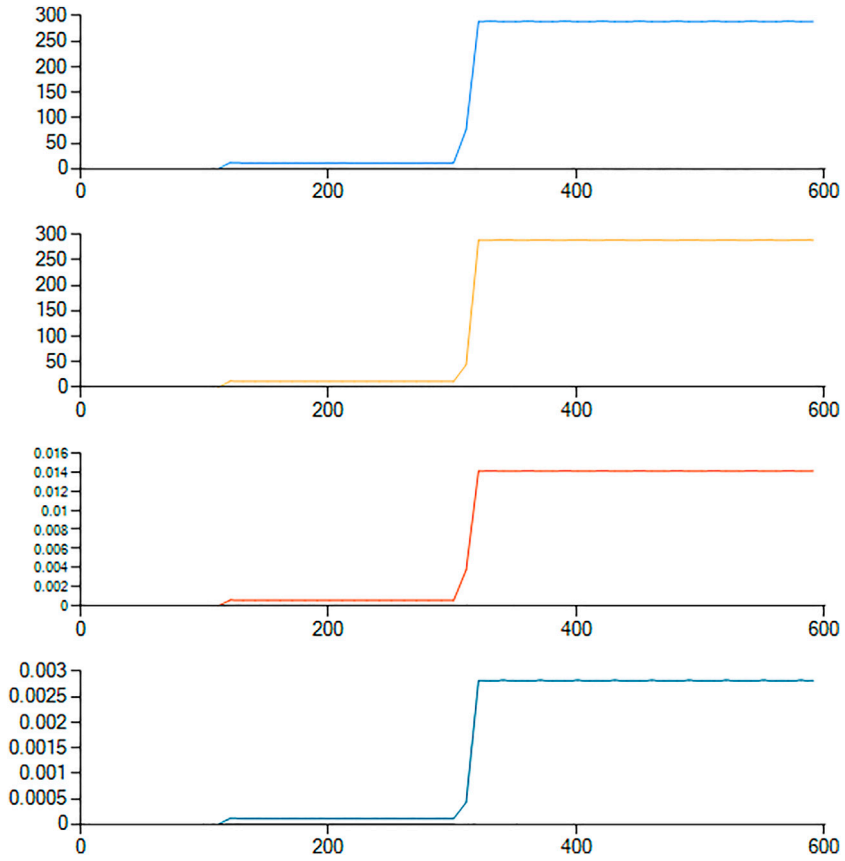

FIGURE 10
Link to ground transmission capability between UAV group 1 and the BeiDou satellite.

$$J<0,\varepsilon\left[\int_0^\infty z^T(t)z(t)dt\right]\le\gamma^2\varepsilon\left[\int_0^\infty w^T(t)v(t)dt\right]$$

According to Definition 5.2, system (21) satisfies H_∞ performance.

In summary, system (24) is stable and satisfies H_∞ performance γ when Eq. 29 is established.

6 Simulations of the stability, anti-interference, information coverage, and transmission capacity of UAVs in power patrol

To verify the performance index and anti-interference performance of the robust fault-tolerant controller for uncertain random time-delay networks, simulation tests are carried out in the MATLAB/Simulink environment [23]. The initial state of the four-rotor UAV was: $x(0) = [\underset{\wedge}{0}\ 0\ 0\ 0\ 0\ 0]$, with an initial value of robust fault tolerance of $k_3\ (0) = 1.9698$, Finally the control parameters of stochastic uncertain networks were $v(t) = 2.581 + e^{-0.0248t}$, $h(t) = e^{-10.24t}$, $\alpha = 100$, $\rho_i = 0.1$, and $\overline{\rho_i} = 0.9$.

According to the UAV model, the simulation results—assuming expected pitch, roll, and yaw angles of 0.8°, 0.5°, and 0.3°, respectively—are represented in the simulation diagram shown in Figure 6.

As shown in Figure 6, in the initial operation phase, the system is in the initial state, with regulation of the robust adaptive fault-tolerant controller. In a very short period of dynamic adjustment, the pitch, roll, and yaw angles can accurately track the desired output of the system (Bi et al., 2021).

Next, to investigate the anti-jamming performance of the designed controller, we assumed pitch, roll, and yaw angles of 0.8°, 0.5°, and 0.3° respectively, and considered the following interference patterns:

Interference pattern 1: We assume that the UAV flight system is subject to external disturbances in the first 5 s, such as strong winds, which are added as a step signal with a magnitude of 0.1. After 5 s, the external disturbance ends and

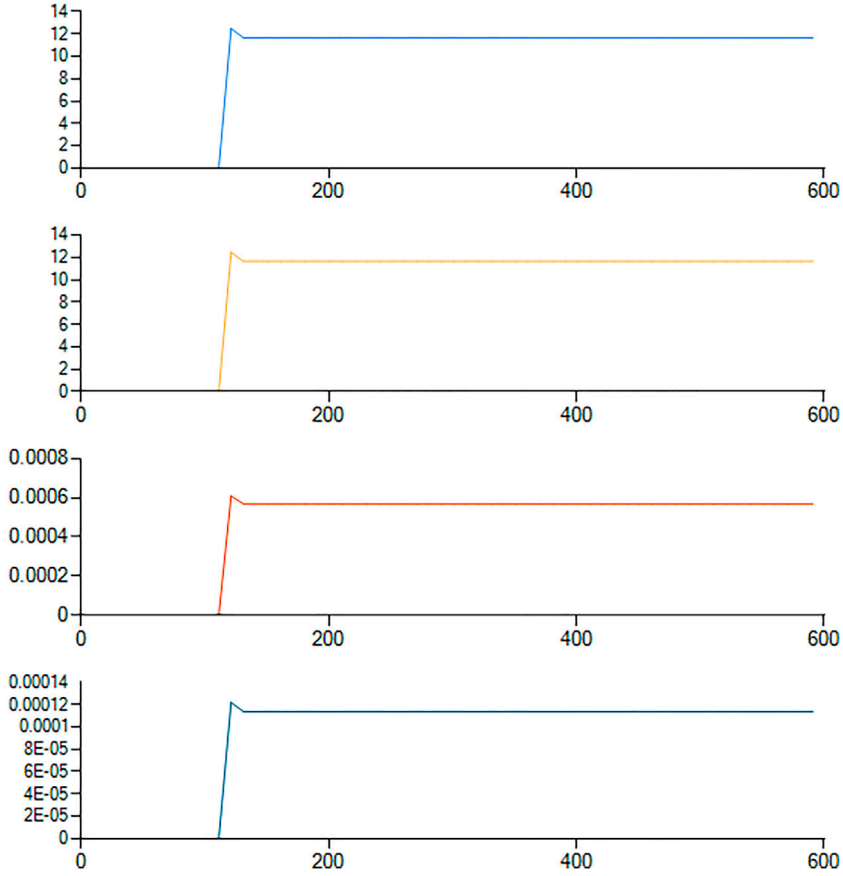

FIGURE 11
Link to ground transmission capability between UAV group 2 and the BeiDou satellite.

the third actuator breaks down. Then, at 10 s, the third actuator experiences a drift fault, drifting to $0.81 + 0.81e^{-t}$, and the fault continues. We obtained the simulation diagram shown in Figure 7.

As shown in Figure 7, before the initial 5 s run, we added a step signal with a magnitude of 0.1 to represent an external disturbance in the system; the system will adjust with short dynamic regulation of the robust adaptive fault-tolerant controller to a steady state. At 5 s, we chose the third actuator to break down, while a drift fault occurred at 10 s. The diagram shows that the system is asymptotically stable, with the adaptive fault-tolerant performance of the designed controller. The elevation, roll, and yaw angles can accurately achieve the desired values of the system, with almost no fluctuation curve, which indicates the good performance of the designed robust adaptive fault-tolerant controller in interference pattern 1(Wang et al., 2019).

Interference pattern 2: Like interference pattern 1, the flight system of the UAV is subjected to an external disturbance in the first 5 s, with an external disturbance amplitude step signal of 0.1. After 5 s, the third actuator experiences a failure and the time-varying partial failure expression is given by $\rho_{\Delta}(t) = 0.1t$, until failure at 70%. Then, at 10 s, the third actuator experiences a drift fault and drifts to $0.81 + 0.81e^{-t}$. Furthermore, the two failures will continue, as represented in the simulation diagram shown in Figure 8.

As shown in Figure 8, before the initial 5 s run, we added a step signal with a magnitude of 0.1 to represent an external disturbance in the system; the system will adjust with short dynamic regulation of the robust adaptive fault-tolerant controller to a steady state. At 5 s, we chose the third actuator to break down, and a drift fault occurred at 10 s. The diagram shows that the system is asymptotically stable, with the adaptive fault-tolerant performance of the designed controller. The elevation, roll, and yaw angles can accurately achieve the desired value of the system, with almost no fluctuation curve, which indicates the good performance of the designed robust adaptive fault-tolerant controller in interference pattern 2 (Wang et al., 2021c).

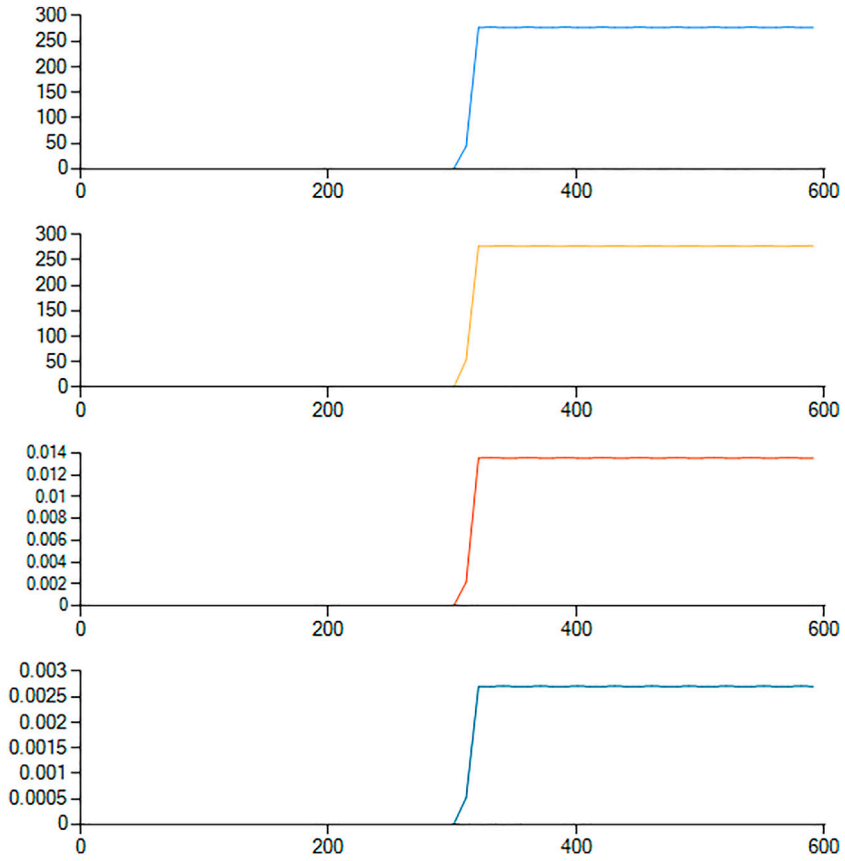

FIGURE 12
Link to ground transmission capability between UAV group 3 and the BeiDou satellite.

In future power inspection processes, patrol UAVs will not only face physical hard-kill but also soft-kill interference, which will cause some losses. Therefore, we need to design a controller to communicate interference suppression, to ensure that the UAV can transmit information and coverage after experiencing communication interference.

First, data comparison and calculation allow evaluation of the information transmission capacity and coverage ability of the four-rotor UAVs. The evaluation results of each index are shown in Table 1 (Wang et al., 2022b).

In the next test, we first assessed the transmission capacity of the network and used the throughput to measure the performance. Figure 11 shows that the throughput of the normal working phase of the system dynamically changes at 0–80 kb/s. After a jump, the system stabilizes at 10–90 kb/s. Compared to the previous process, performance is optimized. Thus, the robust fault-tolerant controller, for uncertain networks with stochastic time delays, showed good optimization performance and can guarantee stable signal transmission capability (Wang et al., 2022c).

Through the above bedding, we tested the UAV information transmission and coverage capacities. We first considered the ground transmission capacity between three UAVs and the BeiDou satellite. Transmission capacity refers to the uplink rate, downlink rate, uplink utilization, and downlink utilization of four indicators.

Figures 9, 10, and 12 show that after the UAV communication is disturbed, the optimal transmission path can be independently selected to ensure capable transmission of the signal, by adjusting the random delay fault-tolerant controller. Thus, the designed controller can reverse information and communication interference.

The results of the data analysis showed that the signal coverage of patrol UAVs under unknown information communication interference could be maintained at approximately 78.4%. The coverage performance of information communication is shown in Figure 13:

Figure 13 shows that after the UAV communication is disturbed, the optimal transmission path can be independently selected to ensure capable transmission of the signal, by adjusting the random delay fault-tolerant controller. Moreover, the global coverage of the signal also showed good improvement (the blue area indicates that the signal is completely covered, while the '+' symbol indicates good coverage performance). Hence, the

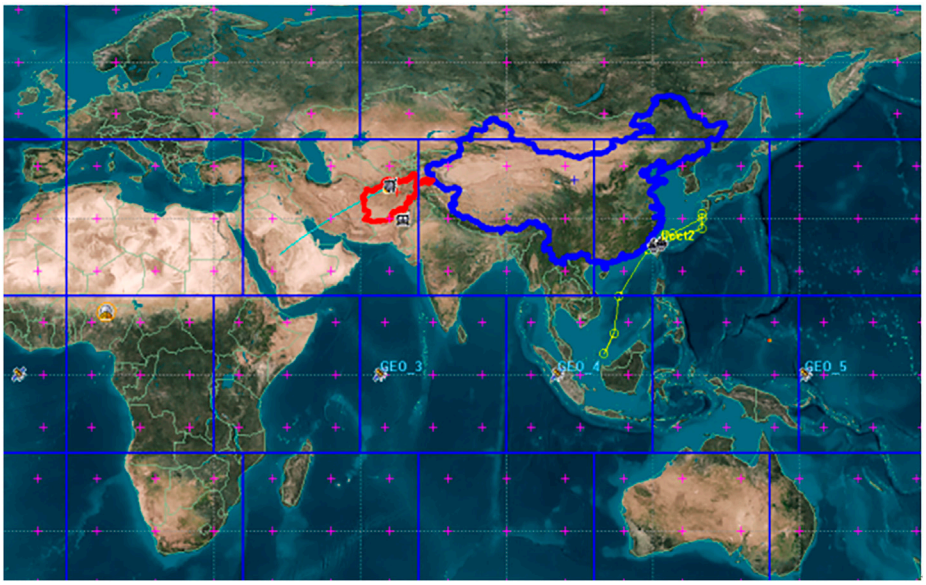

FIGURE 13
UAV group communication coverage performance.

designed controller demonstrated anti-interference ability in information communication.

We also tested the measurement error and compared it to the other results. To make the measurement more obvious, the error in the measurement was sufficiently large. After employing an extended Kalman filter (EKF) in the target tracking scenario, the error was minimized. Compared to the other algorithm, the EFK reduced the noise effect in target tracking. The EKF also effectively helped estimate the target position in the presence of noise and faults. This approach applied the EKF in parallel with fault tolerance algorithms to address the noise. Acceptable results, with a bias less than 5%, demonstrated the performance of the proposed scheme.

This project was used for line inspection of the Zhangjiakou Wind Power Test Base of the State Grid of China. The wind farm covers an area of 10 square kilometers and previously lacked wireless communication coverage. As the data transmission capacity of satellite communication is limited, we adopted a patrol method combining satellite navigation and positioning of the UAV cluster. The results of our experiments showed that the UAVs could transmit data and images, with a data transmission rate of over 50 Mbps. Moreover, the UAV group operated according to the set inspection track, with a deviation range of 2 m, ensuring normal operation of the wind farm.

7 Conclusion

This study established a mathematical model for electrical inspection, using a four-rotor unmanned aerial vehicle. According to the theory of robust adaptive fault-tolerant control, we designed a robust fault-tolerant controller for uncertain networks with random delays. We then performed a control simulation and a test simulation under the conditions of interruption, partial failure, and actuator drift fault. The simulation results showed that the aircraft gradually recovered to the steady-state after interference and failure. During operation, the pitch, roll, and yaw angles of the aircraft met the basic stability requirements and the aircraft stabilized rapidly. Overall, a precise control effect was achieved, and the aircraft demonstrated an anti-communication interference ability. Moreover, the information transfer capability and the global coverage capacity of the UAV also improved. Finally, the simulation results verified that the robust fault-tolerant controller was consistent with the Lyapunov asymptotic stability principle, and demonstrated validity, reliability, accuracy, and practicability.

Data availability statement

The original contributions presented in the study are included in the article/supplementary material, Further inquiries can be directed to the corresponding author.

Author contributions

All authors have made substantial, direct, and intellectual contributions to the work, and have approved its publication.

Funding

This paper was supported by a national grid key project: Key technology of scale engineering application of power battery for echelon utilization (project no. 52010119002F).

Conflict of interest

JS, JW, and YW are employed by State Grid Jibei Zhangjiakou Wind and Solar Energy Storage and Transportation New Energy Co, Ltd.

The remaining authors declare that the research was conducted in the absence of any commercial or financial relationships that could be construed as a potential conflict of interest.

Publisher's note

All claims expressed in this article are solely those of the authors and do not necessarily represent those of their affiliated organizations, or those of the publisher, the editors, and the reviewers. Any product that may be evaluated in this article, or claim that may be made by its manufacturer, are not guaranteed or endorsed by the publisher.

References

Bi, K., Yu, J., Wang, Z., Zhu, W., and Wang, L. (2021). "A high-gain and broadband sector-shaped double-sided printed dipole array antenna for ad-hoc network nodes," in 2021 IEEE MTT-S International Wireless Symposium (IWS), Nanjing, China, 23-26 May 2021 (IEEE), 1–3. doi:10.1109/IWS52775.2021.9499628

Bouadi, H., Bouchoucha, M., and Tadjine, M. (2008). Sliding mode control based on backstepping[J]. *Int. J. Appl. Math. Comput. Sci.* 4 (1), 12–17.

Fei, L. (2014). *Four rotors helicopter adaptive fault-tolerant control algorithm of the attitude control system research[D]*. Nanjing: NUAA.

Hu, S. S. (2013). *Automatic control theory[M]*. Beijing: Science press.

Ioannou, P. A., and Sun, J. (1996). *Robust adaptive control[M]*. Upper Saddle River, NJ: Prentice-Hall, 90–134.

Khosravian, A., and Namvar, M. (2012). Rigid body attitude control using a single vector measurement and gyro. *IEEE Trans. Autom. Contr.* 57 (57), 1273–1279. doi:10.1109/tac.2011.2174663

Liu, L. L. (2009). *Four-rotor modeling and control methods of research of flight simulator*. Changsha: Central south university, 6–9.

Mokhtari, A., Benallegue, A., and Belaidi, A. (2005). Polynomial linear quadratic Gaussian and sliding mode observer for a quadrotor unmanned aerial vehicle[J]. *J. Robotics Mechatronics* 17 (4), 43–47.

Qing, Y., Song, H., Zhao, Q., and Shi, L. (2009). *Four-rotor aircraft modeling, control, and simulation*. Naval aeronautical engineering institute.

Tang, M. W., and Dai, L. H. (2013). Application of UAV in power line patrol[J]. *China Electr. Power* 46 (3), 35–38.

Wang, H. Y., Yuan, L. H., and Wu, B. (2009). *MATLAB simulation and design of the control system[M]*. Beijing: Higher education press.

Wang, Z., Yu, J., Lin, S., Dong, J., and Yu, Z. (2021). Distributed robust H∞ adaptive faultfault-tolerant control of amorphous and flat air-to-ground wireless self-organizing network system. *Assem. Autom.* 41 (6), 641–658. doi:10.1108/AA-04-2021-0041

Wang, Z., Yu, J., and Lin, S. (2021). "High-speed mobile real-time topology optimization of amorphous flattened air-to-ground wireless self-organizing network nodes based on dynamic planning," in *2021 3rd international conference on electronics and communication, network and computer technology (ECNCT 2021)* (SPIE Proceedings). doi:10.1117/12.2628545

Wang, Z., Yu, J., and Lin, S. (2022). Research on robust adaptive sliding film fault-tolerant control under nonlinear distortion of signal transmission in amorphous flat air-to-ground wireless ad-hoc network system. *Assem. Autom.* 42, 190–201. doi:10.1108/AA-04-2021-0045

Wang, Z., Yu, J., Wang, Z., and Lin, S. (2022). Bidirectional robust and fault-tolerant H_∞ non-sensitive compensation filter controller based on amorphous flattened air-to-ground wireless self-assembly system. *ISA Trans.* doi:10.1016/j.isatra.2022.05.043

Wang, Z., Dong, J., Yu, J., Yu, Z., Lin, S., and Li, K. (2020). "The air-ground integrated MIMO cooperative relay beamforming wireless ad-hoc network technology research that based on maximum ratio combining," in 2020 International Workshop on Electronic Communication and Artificial Intelligence (IWECAI), Shanghai, China, 12-14 June 2020 (IEEE), 11–19. doi:10.1109/IWECAI50956.2020.00010

Wang, Z. F., and Fu, X. F. (2017). LQR optimal control for quad-rotor aircraft[J]. *Sens. world* 3, 17–23.

Wang, Z. F., Yu, J. G., Bi, K., Lin, S. J., and Yu, Z. (2021). "A 2.4 GHz bidirectional power amplifier extending nodes distance of transmission to 14.8 km for amorphous flat air-to-ground wireless ad hoc network," in *Arabian journal for science and engineering* (Spinger). doi:10.1007/s13369-021-06089-2

Wang, Z. F., Yu, J. G., Bi, K., Lin, S. J., and Yu, Z. (2022). Research on long-distance transmission of nodes in amorphous flat air-to-ground wireless ad-hoc network based on bidirectional relay beamforming. *AD HOC Sens. Wirel. Netw.* 51, 41–59.

Wang, Z. H., and Xiao-Ning, H. (2012). Research on transmission line inspection system based on four - rotor UAV[J]. *China Electr. Power* 10, 59–62.

Wang, Z., Yu, J., Lin, S., Dong, J., and Yu, Z. (2019). Distributed robust adaptive faultfault-tolerant mechanism for quadrotor UAV real-time wireless network systems with random delay and packet loss. *IEEE Access* 7, 134055–134062. doi:10.1109/ACCESS.2019.2936590

Xin-Zhe, Y. (2012). *The four-rotor helicopter attitude system based on state observer active fault tolerant control research[D]*. Nanjing: NUAA.

Yan, D. (2013). Study on the method of UAV robust control. *Mach. automation* 6, 76.

Yang, H. X., Yang, X. X., and Zhang, W. H. (2012). Distributed control of spacecraft formation using improved cyclic pursuit with beacon guidance. *Appl. Mech. Mech. Eng.* 138-139, 38–43. doi:10.4028/www.scientific.net/amm.138-139.38

Yong, Z. (2013). *Four rotors aircraft fault-tolerant control system design and implementation [D]*. Chengdu: UESTC.

Zhang, D. F., Wang, Z. Q., and Han, X. Dg (2014). *Satisfactory Fault-Tolerant contro [M]*. Beijing: Science press.

Zheng, J. X., Yuan, Z. H., and Yan-Ping, L. (2014). *Adaptive fault-tolerant control theory method[M]*. Beijing: Electronic industry press.

Zheng, J. X., Yang, G. H., Xiao-huan, C., and Wei-wei, C. (2013). Robust H∞ fault-tolerant control systems and adaptive compensation design[J]. *Acta autom.* 39 (1), 31–42. doi:10.1016/S1874-1029(13)60004-X